



OPEN ACCESS

EDITED BY

Shaohong Xia,
South China Sea Institute of
Oceanology (CAS), China

REVIEWED BY

Jiangyang Zhang,
South China Sea Institute of
Oceanology (CAS), China
Chao Lei,
China University of Geosciences
Wuhan, China

*CORRESPONDENCE

Jie Liao,
liaojie5@mail.sysu.edu.cn

SPECIALTY SECTION

This article was submitted to Solid Earth
Geophysics,
a section of the journal
Frontiers in Earth Science

RECEIVED 27 September 2022

ACCEPTED 14 November 2022

PUBLISHED 20 January 2023

CITATION

Li H, Liao J, Shen Y, Qing J, Wu Y, Zhao Z
and Shi X (2023), Rifting/spreading
propagation interacts with preexisting
transform faults: 3D
geodynamic modeling.
Front. Earth Sci. 10:1054747.
doi: 10.3389/feart.2022.1054747

COPYRIGHT

© 2023 Li, Liao, Shen, Qing, Wu, Zhao
and Shi. This is an open-access article
distributed under the terms of the
[Creative Commons Attribution License
\(CC BY\)](https://creativecommons.org/licenses/by/4.0/). The use, distribution or
reproduction in other forums is
permitted, provided the original
author(s) and the copyright owner(s) are
credited and that the original
publication in this journal is cited, in
accordance with accepted academic
practice. No use, distribution or
reproduction is permitted which does
not comply with these terms.

Rifting/spreading propagation interacts with preexisting transform faults: 3D geodynamic modeling

Hao Li¹, Jie Liao^{1,2,3*}, Yongqiang Shen¹, Jiarong Qing¹,
Yangming Wu¹, Zhongxian Zhao⁴ and Xiaobin Shi⁴

¹School of Earth Sciences and Engineering, Sun Yat-Sen University, Guangzhou, China, ²Southern Marine Science and Engineering Guangdong Laboratory (Zhuhai), Zhuhai, China, ³Guangdong Provincial Key Lab of Geodynamics and Geohazards, Guangzhou, China, ⁴Key Laboratory of Ocean and Marginal Sea Geology, South China Sea Institute of Oceanology, Chinese Academy of Sciences, Guangzhou, China

The divergent rifting/spreading centers and the strike-slip transform faults are the essential tectonic units on Earth, the dynamic evolution of which regulates the development of rifting/spreading basins. The propagation of rifting/spreading centers may interact with pre-existing transform faults, but how they interact with each other remains enigmatic. Here we use three-dimensional geodynamical numeric models to systematically simulate the interaction between rifting/spreading propagation and the pre-existing transform faults. Our model results provide the following findings. 1) The pre-existing transform faults affect rifting/spreading propagation promoting the formation of ridge segments with an offset distance, facilitating the process of spreading of the western sea basin and restraining the propagation of the east sea basin. Yet, the evolution of the transform faults is regulated by rifting/spreading propagation, featured by the increase of its length, the change in its width along strike and the presence of lineated magmatism. 2) The initial length and orientation of the pre-existing transform faults largely affect rifting/spreading propagation, i.e., large transform fault length favors the formation of large offset between ridge segments, and oblique transform faults facilitate the formation of overlapped spreading centers. 3) Model results shed new light on the evolution of the South China Sea basin, implying that the observed ridge segments in the east and southwest sub-basins, the difference of the Zhongnan Fault Zone width along strike and the lineated volcanos along the Zhongnan Fault Zone are the results of the interaction between the rifting/spreading propagation and the pre-existing transform fault.

KEYWORDS

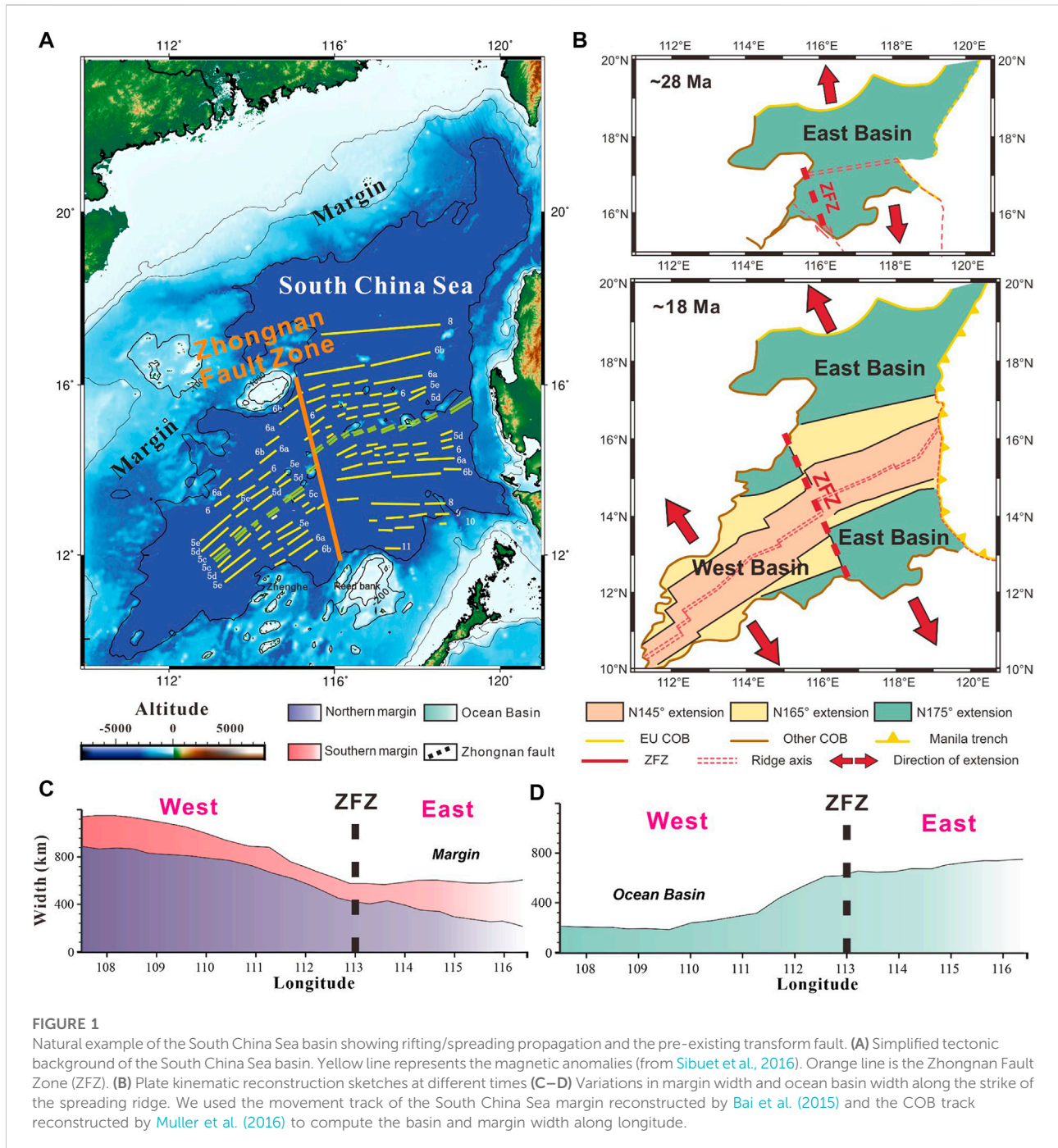
rifting/spreading propagation, pre-existing transform faults, geodynamic modeling, South China Sea, Zhongnan Fault Zone

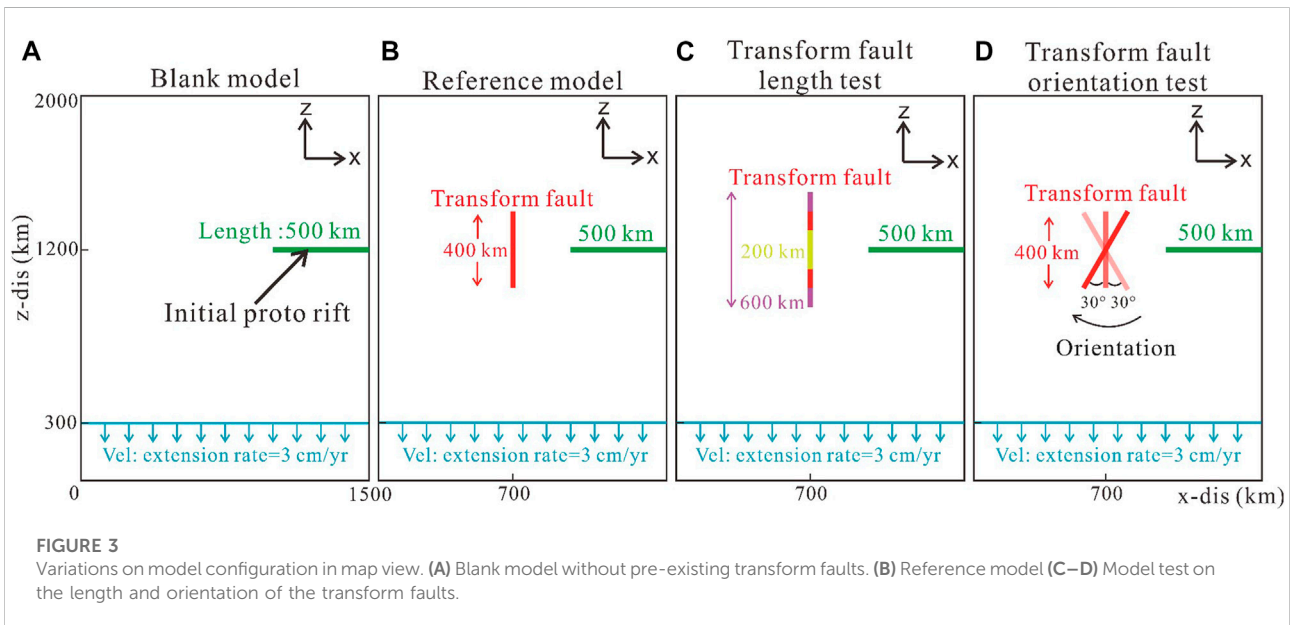
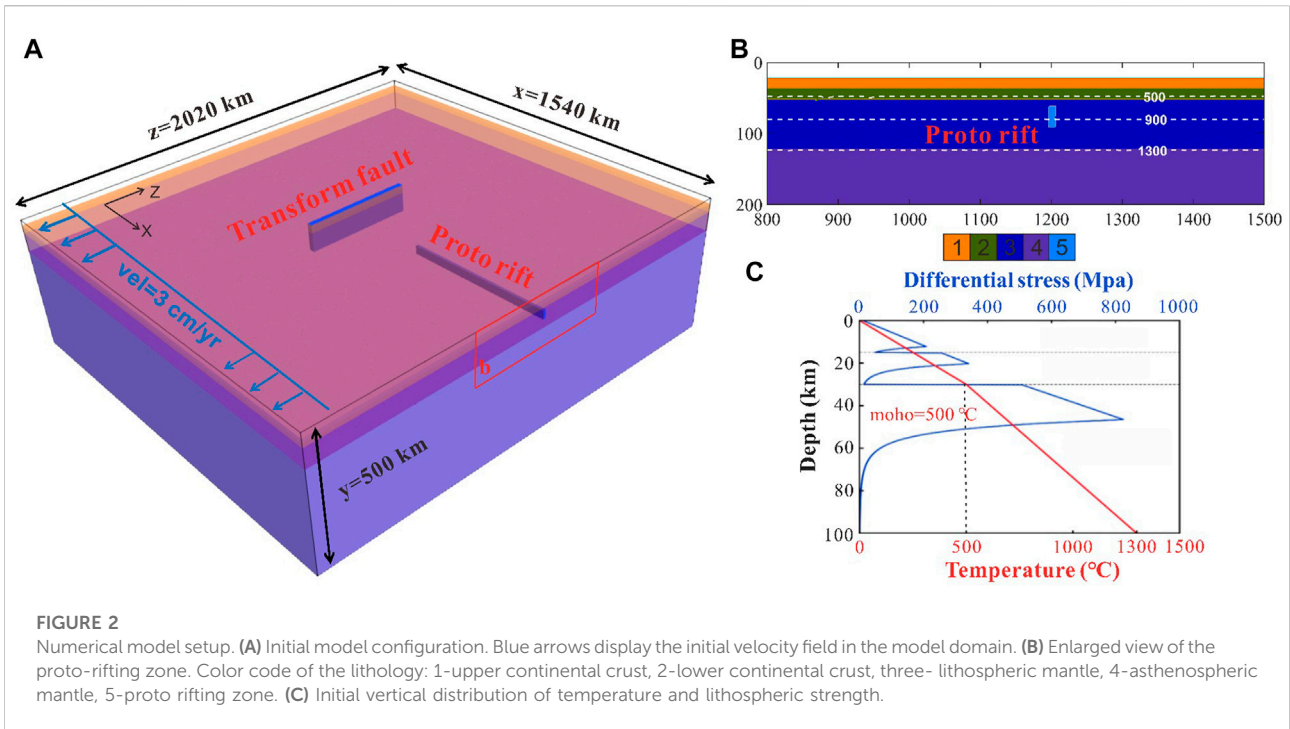
Introduction

Rifting/spreading centers and (continental/oceanic) transform faults are essential tectonic units affecting lithosphere dynamics. These two tectonic units are not isolated in nature but often show intensive interactions. A possible interaction between the two units is how the pre-existing transform faults interact with rifting/spreading propagation, as observed in many natural examples (e.g., the

South China Sea basin). Individual process of either transform fault evolution or rifting/spreading propagation is largely investigated in previous studies (e.g., Hey et al., 1980; Courtillot, 1982; Vink, 1982; Gerya, 2013; Le Pourhiet et al., 2017; Illsley-Kemp et al., 2018; Le Pourhiet et al., 2018), but the interaction between rifting/spreading propagation and pre-existing transform faults remains poorly understood.

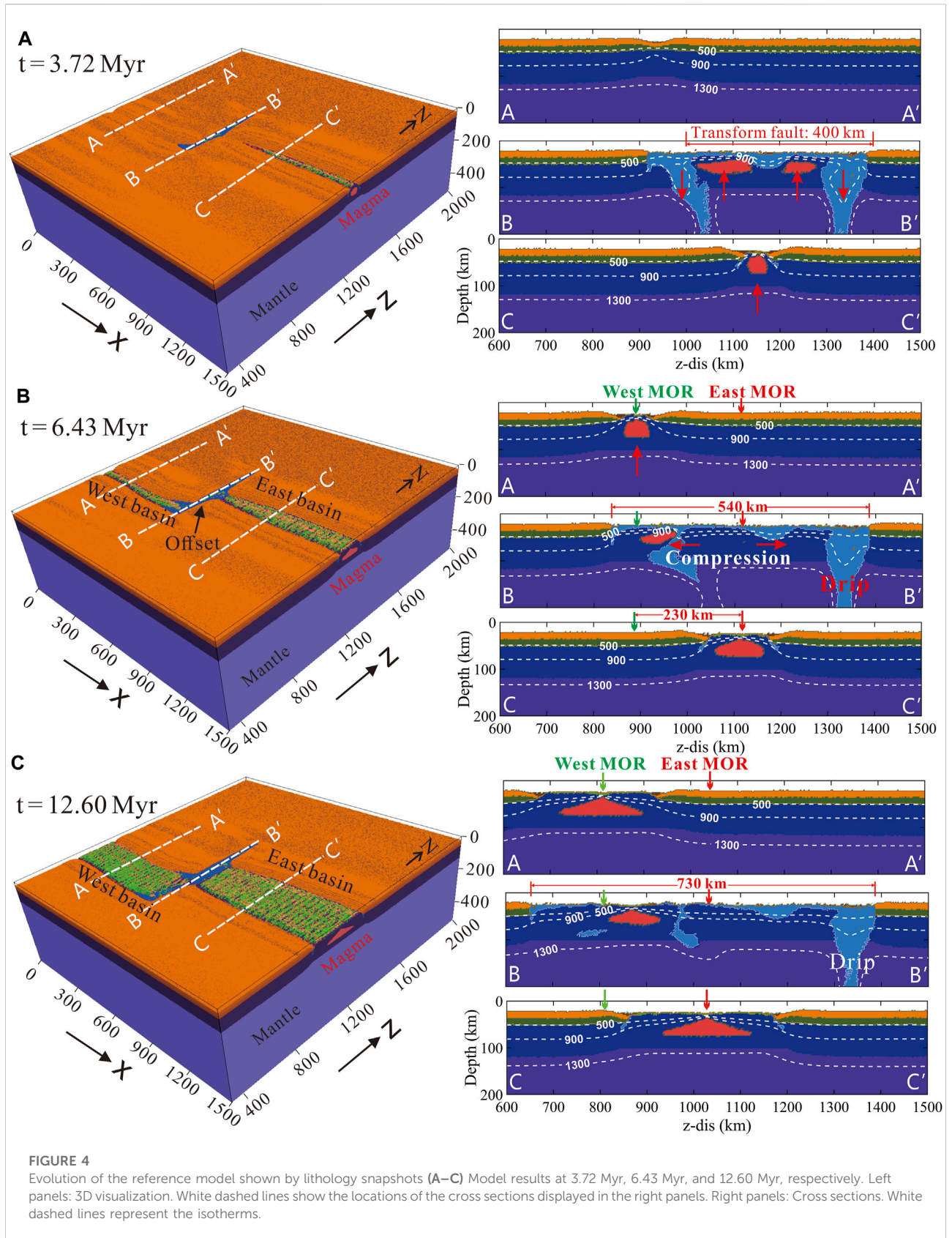
The South China Sea basin is a possible example showing rifting/spreading propagation interacted by the pre-existing

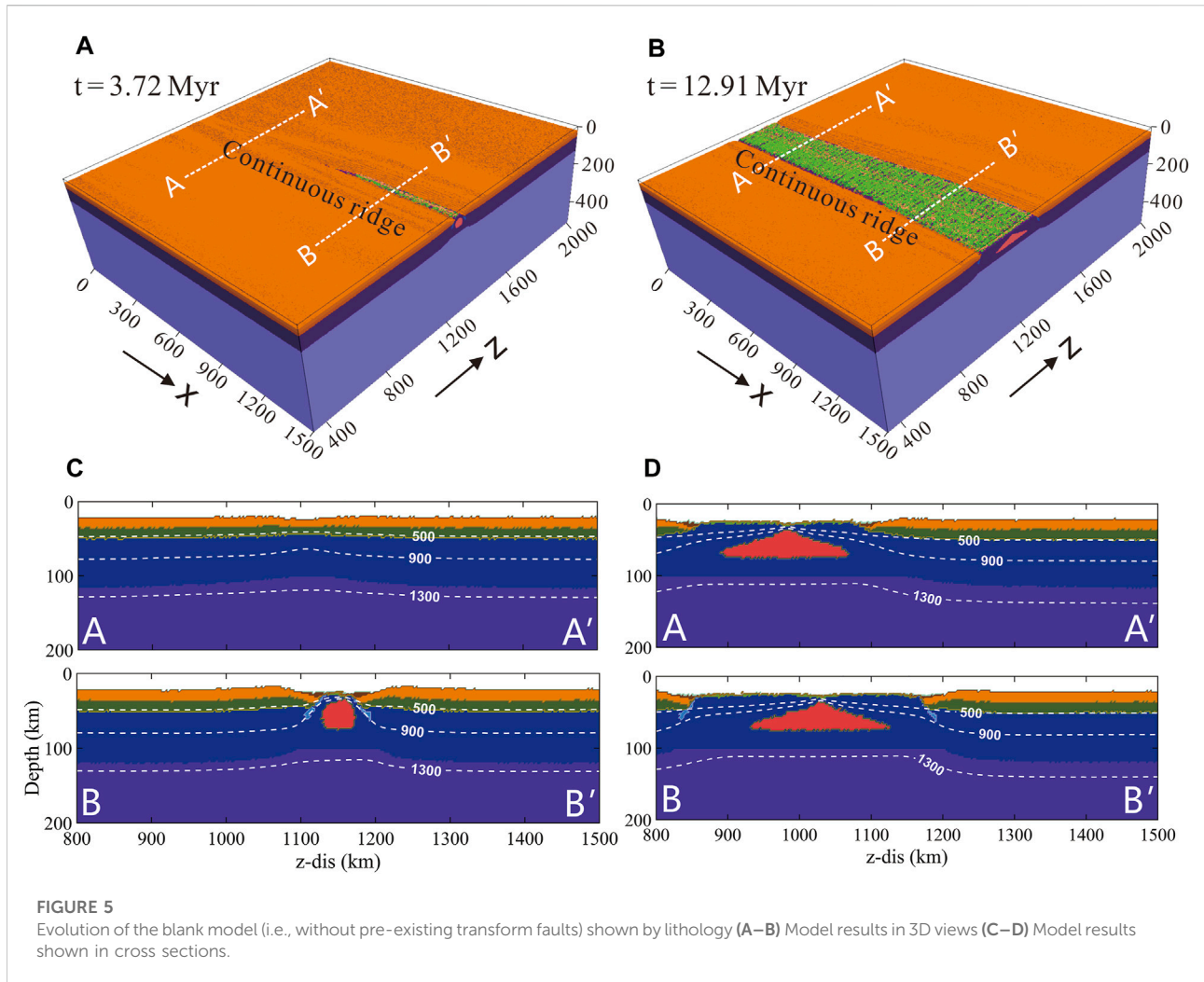




Zhongnan Fault Zone (Figure 1A), which evolved from a continental transform fault in the rifting stage to an oceanic transform fault in the spreading stage since. The South China Sea basin spreading started at ~32 Ma and terminated at ~15 Ma (Briais et al., 1993; Li et al., 2012; Sibuet et al., 2016), and the spreading process is largely three-dimensional with strong lateral variations. The spreading ridge of the South China Sea basin

propagated from east to west (Figure 1B), with decreasing oceanic basin width from east to west (Figures 1C, D). The Zhongnan Fault Zone is a boundary separating the east ocean basin from the west (Barckhausen et al., 2004; Li et al., 2008; Li et al., 2012, 2014; Barckhausen and Roeser, 2014). Although the age of the Zhongnan Fault Zone is debated (Tongkul et al., 1993; Li et al., 2008; Yan, 2008; Li et al., 2012; Li et al., 2014; Ruan et al.,





2016; Sibuet et al., 2016), increasing studies proposed that the Zhongnan Fault Zone was formed before the South China Sea basin spreading (Briais et al., 1993; Yan, 2008; Sibuet et al., 2016; Li et al., 2017). The recent studies using seismic reflection data demonstrated that the Zhongnan Fault Zone developed before the opening of the South China Sea basin (Li et al., 2017; Xu et al., 2019, Xu et al., 2021).

This study investigates systematically how pre-existing transform faults interact with rifting/spreading propagation using a three-dimensional thermomechanical coupled numeric model. The model results suggest that the pre-existing transform faults strongly interact with rifting/spreading propagation, forming discontinuous ridge segments and promoting the growth of transform faults. Our results shed new light on the dynamic evolution of rifting/spreading propagation and transform fault growth in the South China Sea basin.

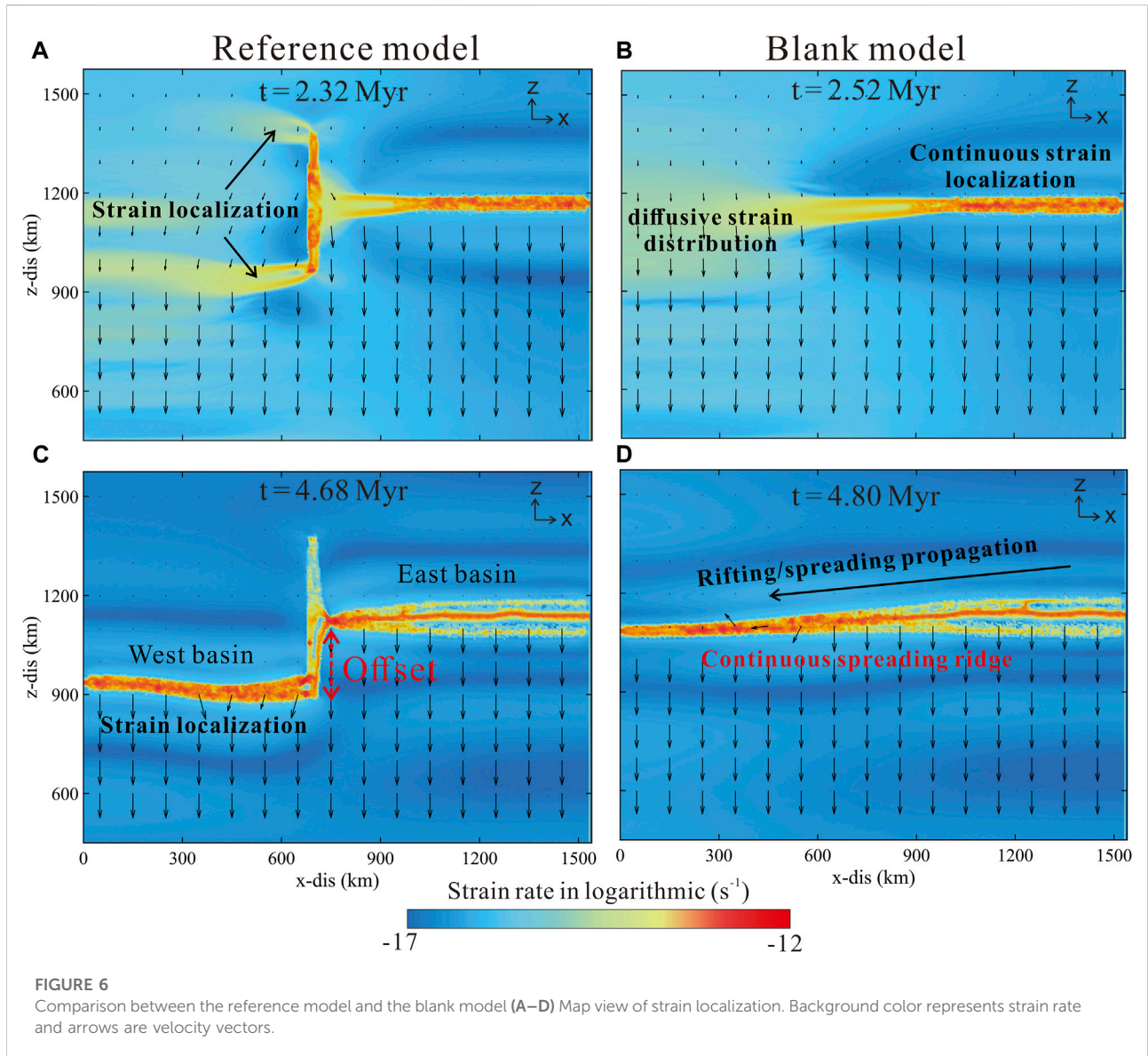
Methods

Numerical methods

We use the 3D thermomechanical code I3ELVIS (Gerya and Yuen, 2003; Gerya, 2013) to conduct numerical simulations. The code solves the three-dimensional mass conservation equation (incompressible medium), momentum conservation equation, and energy conservation equation using the finite difference algorithm. The Stokes flow is coupled with the time-dependent heat conservation equation. The following three governing equations (i.e., the mass, momentum and energy conservation equations) are solved in the numerical code:

$$\text{div}(v_i) = \frac{\partial v_i}{\partial x_i} = 0$$

$$\frac{\partial \sigma'_{ij}}{\partial x_j} = \frac{\partial P}{\partial x_i} - g\rho(C, M, P, T)$$



$$\rho C_p \left(\frac{dT}{dt} \right) = \frac{\partial}{\partial x_i} \left(k \frac{\partial T}{\partial x_i} \right) + H$$

where v_i is the velocity vector, ρ is the density of rock, which changes with rock parameters, g is gravitational acceleration, σ'_{ij} is the deviatoric stress tensor, σ_{xi} is the shear stress tensor, C_p is isobaric heat capacity, dT/dt is the partial derivative of temperature T with respect to time T , k is the thermal conductivity, which is affected by temperature T , pressure P and rock type C , H represents internal heat source, including radioactive heat source, shear heat source, adiabatic pressure heat source and phase change heat source (Burg and Gerya, 2005).

The numerical simulation program in this study integrates the rheological relationship of the strain rate with the viscoplastic constitutive relationship to calculate the deviatoric stress

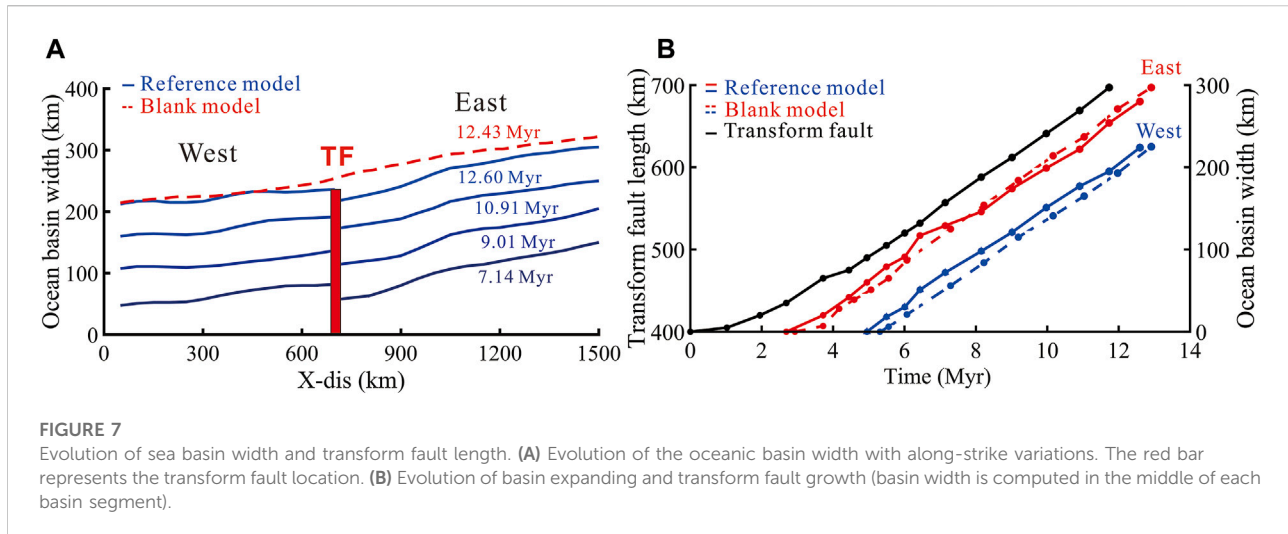
tensor. Plastic rheology is described by the Drucker–Prager yield criterion, where the yield stress (σ_{yield}) is pressure-dependent (C is rock cohesion, φ is internal friction angle and λ is the pore fluid coefficient). Viscosity due to plastic deformation ($\eta_{plastic}$) is computed based on the square root of the second invariant of strain rate ($\dot{\epsilon}_{II}$). Eventually, the effective viscosity of rocks (η_{eff}) is constrained by both viscous and plastic deformation.

$$\eta_{ductile} = \dot{\epsilon}_{II}^{\frac{1-n}{n}} A^{\frac{1}{n}} \exp\left(\frac{E_a + PV_a}{nRT}\right)$$

$$\sigma_{yield} = C_0 + P \sin(\varphi) (1 - \lambda)$$

$$\eta_{plastic} = \frac{\sigma_{yield}}{2\dot{\epsilon}_{II}}$$

$$\eta_{eff} = \min(\eta_{ductile}, \eta_{plastic})$$



In the simulation, rock deformation and material migration are solved by marker-in-cell method. The rock deformation (nonlinear visco-plastic deformation) of each layer is controlled by the rheological properties of different lithology. In addition, partial melting, plate dehydration, water migration and mineral phase transformation are introduced into the calculation program to simulate the various processes of natural tectonic movement.

Model setup

The physical dimension of our models is $2,020 \text{ km} \times 1,540 \text{ km} \times 500 \text{ km}$ (in the order of x , y and z directions), with a uniform grid consisting of $308 \times 404 \times 100$ Eulerian nodes. The thickness of the lithosphere in our model is 120 km, with a 15 km thick upper crust and a 15 km thick lower crust. A transform fault with the length of 300 km and the width of 20 km is imposed in the middle of the model domain, parallel to the direction of boundary extension. A proto rifting zone with the length of 500 km and the width of 20 km is employed on the right edge of the model domain, which evolves to a mature rifting and spreading center. Different lithological compositions are employed to control the initial physical and chemical properties in the model. Wet quartzite and felsic granulite are applied for the continental upper and lower crust, respectively. Dry olivine is used for the lithospheric and asthenospheric mantle. Wet Olivine that has weak rheological properties is employed to the transform fault zone and the proto rifting zone. In addition, a layer of 'sticky' air (viscosity of 10^{18} Pa s) is applied above the crust which allows the surface of the crust to deform freely and spontaneously (Cramer et al., 2012).

A linear temperature structure is employed for the lithosphere. The temperature increases linearly from 273 K at the surface (20 km) to 773 K at the moho surface (50 km) and increases

linearly from the moho to 1573 K at the lithosphere and asthenosphere boundary (120 km). The asthenospheric mantle is adiabatic with thermal gradient of $0.5^\circ\text{C}/\text{km}$. Constant temperature is applied at the top and bottom boundaries. The left and right boundaries are thermal isolated with no heat flux across.

Velocity boundary conditions are free slip on all boundaries. Additional internal boundary velocities (e.g., 3 cm/yr in the blank model as well as in the reference model, Figures 2A, 3) are set at the southern boundary at $z = 300 \text{ km}$.

Due to the imposed "sticky air" layer, the crustal surface is roughly described as a free surface and can therefore deform spontaneously. We use simplified erosion and sedimentation method that are independent of topographic slope and local elevation (Burov and Cloetingh, 1997). Constant and moderate erosion and deposition rates (0.315 mm/year) that within the range of natural data are employed. The surface erosion and sedimentation are simulated by resolving the transport equation at the Eulerian node for each time step (Gerya and Yuen, 2003):

$$\frac{\partial y_s}{\partial T} = v_y - v_x \frac{\partial y_s}{\partial x} - v_s + v_e$$

where y_s is the vertical position of the crustal surface, v_y and v_x are the vertical and horizontal velocity components on the crustal surface, v_s and v_e are the rates of sedimentation and erosion, respectively, which correspond to the following relations: $v_s = 0$ and $v_e = 0.315 \text{ mm/yr}$ for $y_s < 20 \text{ km}$, $v_s = 0.315 \text{ mm/yr}$ and $v_e = 0$ for $y_s \geq 20 \text{ km}$ (the initial depth of the crustal surface is 20 km).

We set up a series of geodynamic numerical models to explore the interaction between the pre-existing transform faults and the rifting/spreading propagation (map view of the initial model configuration in terms of the location of the rifting/spreading center and the transform fault; Figure 3). We further run a blank model without pre-existing transform faults to compare rifting/spreading propagation (Figure 3A). Based on

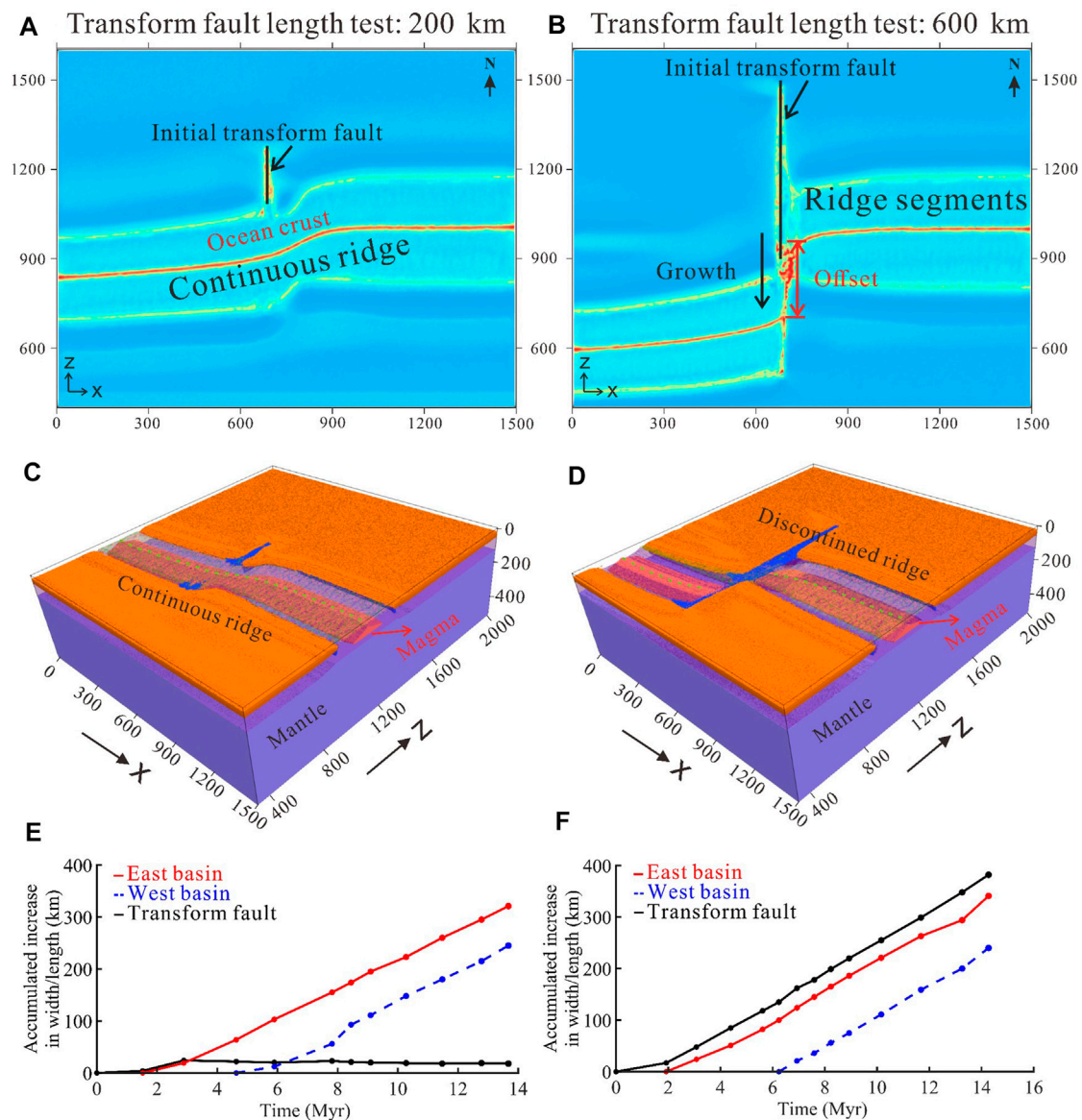


FIGURE 8

Effect of transform fault length (A–B) Map view of viscosity fields (C–D) Lithology field in 3D view. Mid-ocean ridges are indicated by the green dashed lines (E–F) Growth of transform faults and oceanic basins (Data are taken from the middle of the ocean basin and transform fault).

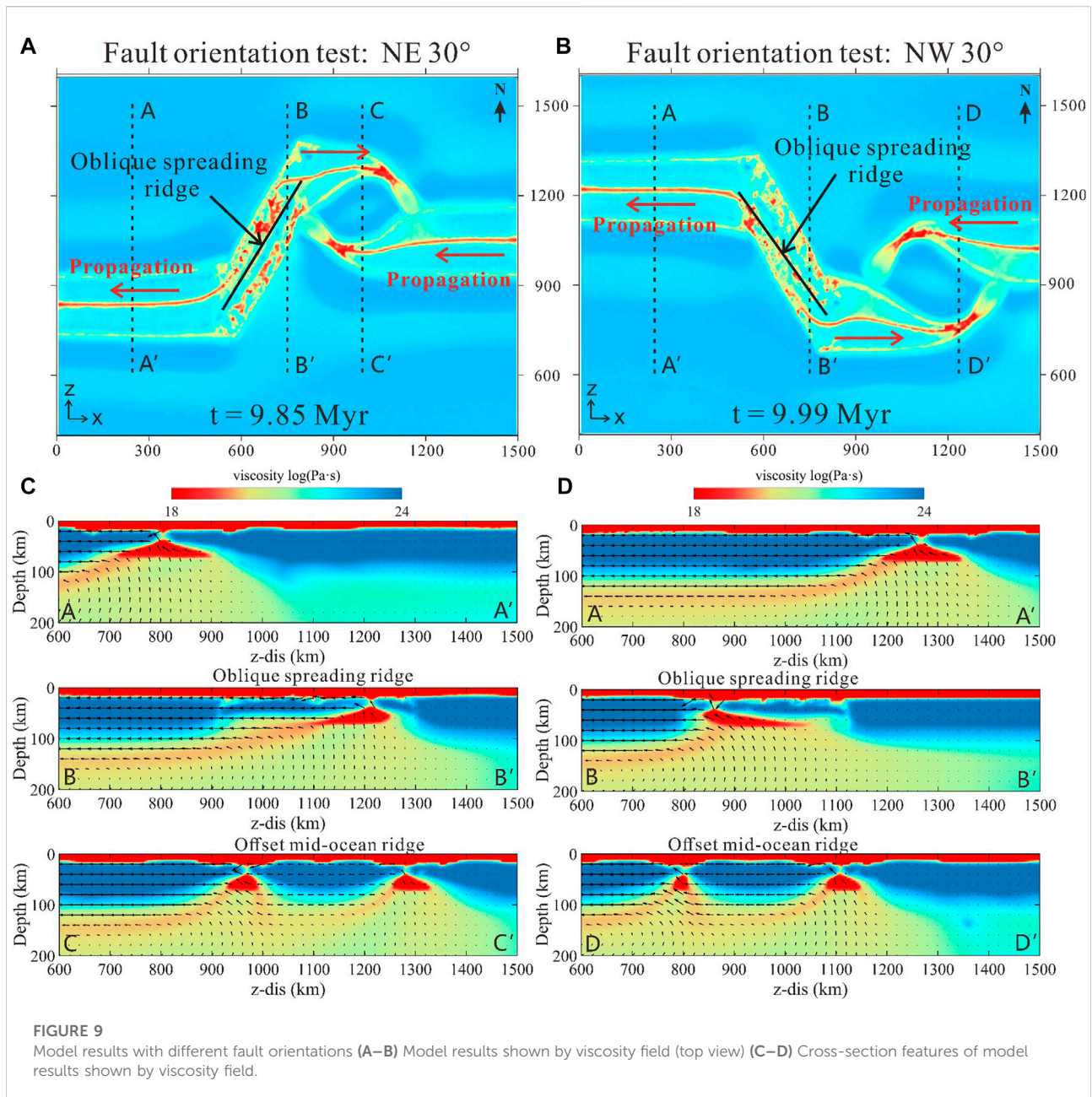
the reference model (Figure 3B), we further investigate parameter effects in terms of the length and orientation of the pre-existing transform fault (Figures 3C,D).

Results

Reference model evolution

We conducted a series of numerical models to investigate the influence of pre-existing transform faults on rifting/

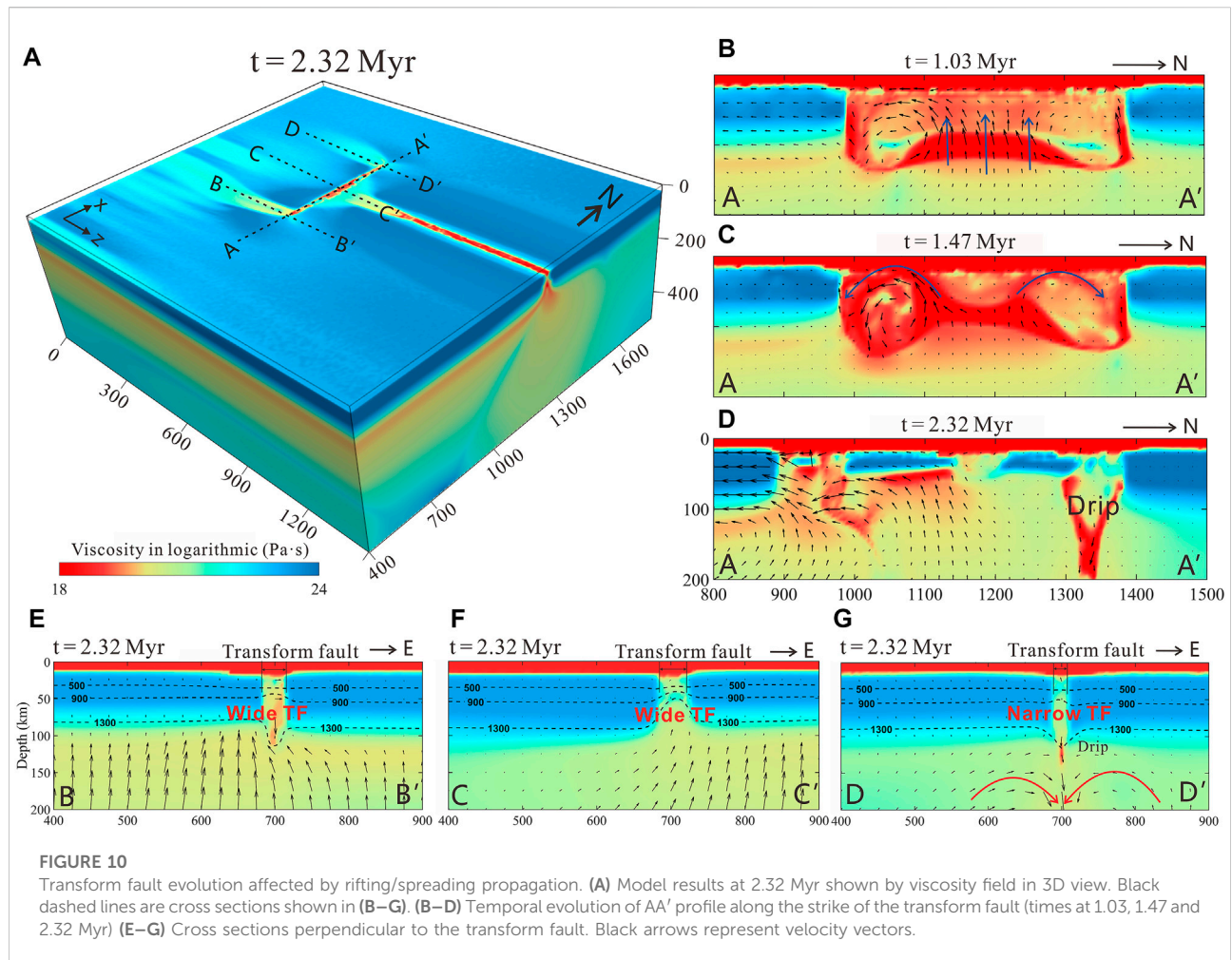
spreading propagation. Typical evolution stages of the reference model are documented (Figure 4 and Supplementary Figure S1). 1) In the early stage, rifting propagation dominates model evolution (Figure 4A). The rifting center is formed along the prescribed proto rifting zone, and propagates laterally. In front of the propagated rifting center, the evolution of the pre-existing transform fault is featured by transtensional deformation in the middle and transpressional deformation at the ends. As a consequence of the transtensional and transpressional deformation, material upwelling and downwelling in the



fault zone is observed, respectively (BB' profile, Figure 4A). 2) With further model evolution, propagation of the rifting/spreading center is affected by the presence of the transform fault, and the remarkable feature is the formation of the two ridge segments with an offset distance (Figure 4B). The younger ridge segment connects the tip of the transform fault, and the offset distance between the two ridge segments is half of the transform fault length. The ridge-transform fault-ridge system is established. 3) In the late stage, steady spreading forms leading to the widening of sea basins. The transform fault grows dramatically with the increase in its

length, from the original length of 400 km to ~730 km at this moment (BB' profile, Figure 4C).

We further run a blank model to investigate the propagation of rifting/spreading centers without the influence of pre-existing transform faults (Figure 5). Similar to the reference model, the rifting/spreading centers first develop along the proto rifting zone, and propagate laterally to the other side of the model domain. The main difference is that a relatively straight and continuous spreading ridge is formed in the blank model, in contrast to the formation of two ridge segments affected by the pre-existing transform fault in the reference model.



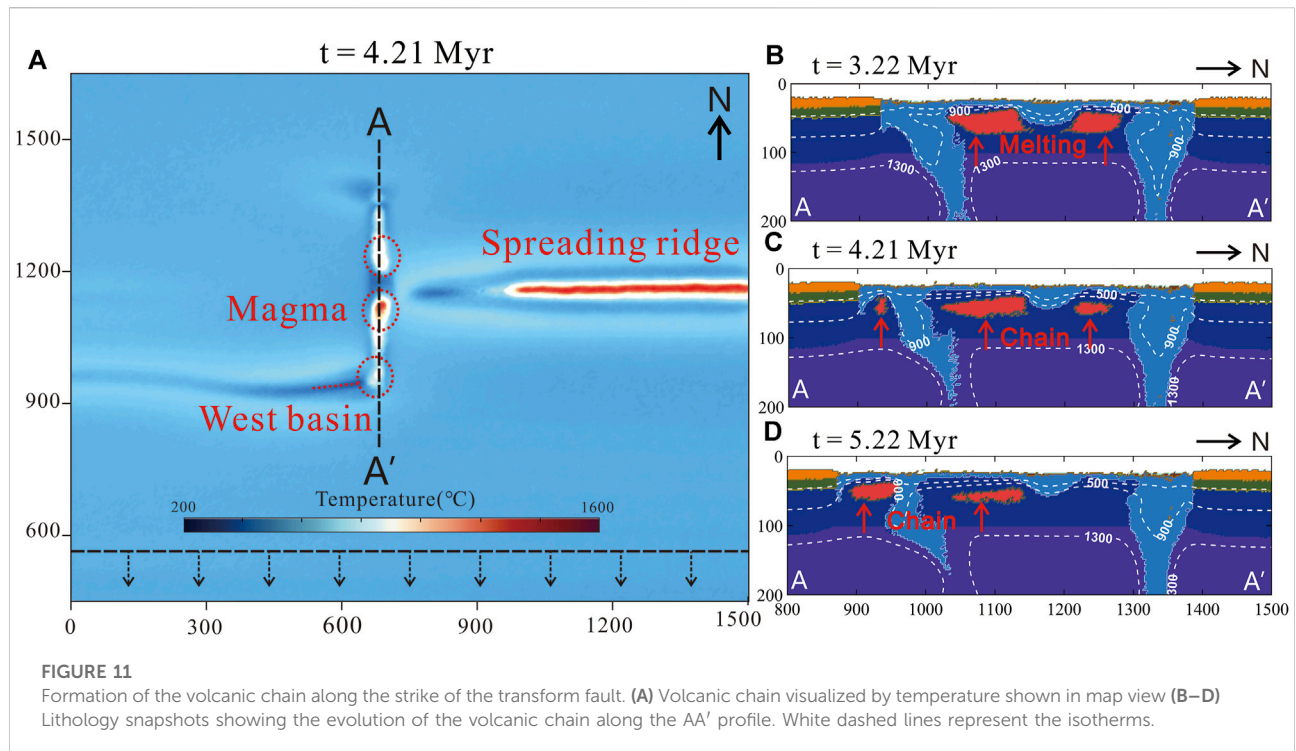
The difference between the two models is further compared in terms of strain rate evolution (Figure 6). In the reference model, the transform fault interacts rifting/spreading propagation, inhibiting the continuous strain localization ahead of the propagated spreading center. Two strain localization zones connecting to the ends of the transform fault are formed (Figure 6A), and the one locates closer to the extensional boundary evolves to a spreading center finally, while the other one becomes abandoned (Figure 6C). In the blank model, strain localization continuously formed ahead of the propagated rifting/spreading center, although diffusive strain distribution is seen in the early stage (Figures 6B,D).

In addition, the extending of the sea basins is computed in the reference model and compared to that in the blank model (Figure 7). The eastern sea basin (separated by the transform fault) is wider than that of the western sea basin since it develops earlier (Figure 7). Gradual decrease in the width of the eastern sea basin is observed (Figure 7A), as a consequence to spreading propagation. The width of the western basin, however, is relatively constant with negligible variation along strike

(Figure 7A). The main reason is the fast strain localization in the western basin facilitated by the southern end of the transform fault. The blank model without the pre-existing transform fault shows a gradual decrease in the width of the sea basin from east to west in the entire model. Besides, the width of the western basin in the reference model is slightly larger than that in the blank model (Figure 7B), suggesting the promotion of the pre-existing transform fault on the development of the western basin.

Influence of transform fault length

We further conduct a series of numerical experiments to study the influence of transform fault length. Based on the reference model (i.e., 400 km of the transform fault length), we test the models with a shorter (i.e., 200 km) and a longer (i.e., 600 km) pre-existing transform fault (Figure 8). In the model with a shorter pre-existing transform fault (i.e., 200 km; Figure 8A), a continuous spreading ridge with slight curvature around the transform fault is formed (Figure 8A). The growth of



the transform fault terminates after the spreading ridge propagating to the fault and breaking the preexisting transform fault (Figure 8E). In the model with a longer transform fault (i.e., 600 km; Figure 8B), however, two ridge segments are formed with a larger offset distance compared to that in the reference model. The transform fault continues to grow with the spreading of the ridge centers (Figure 8F). These differences suggest that long transform faults promote the formation of two separated ridge segments during spreading propagation.

Influence of transform fault orientation

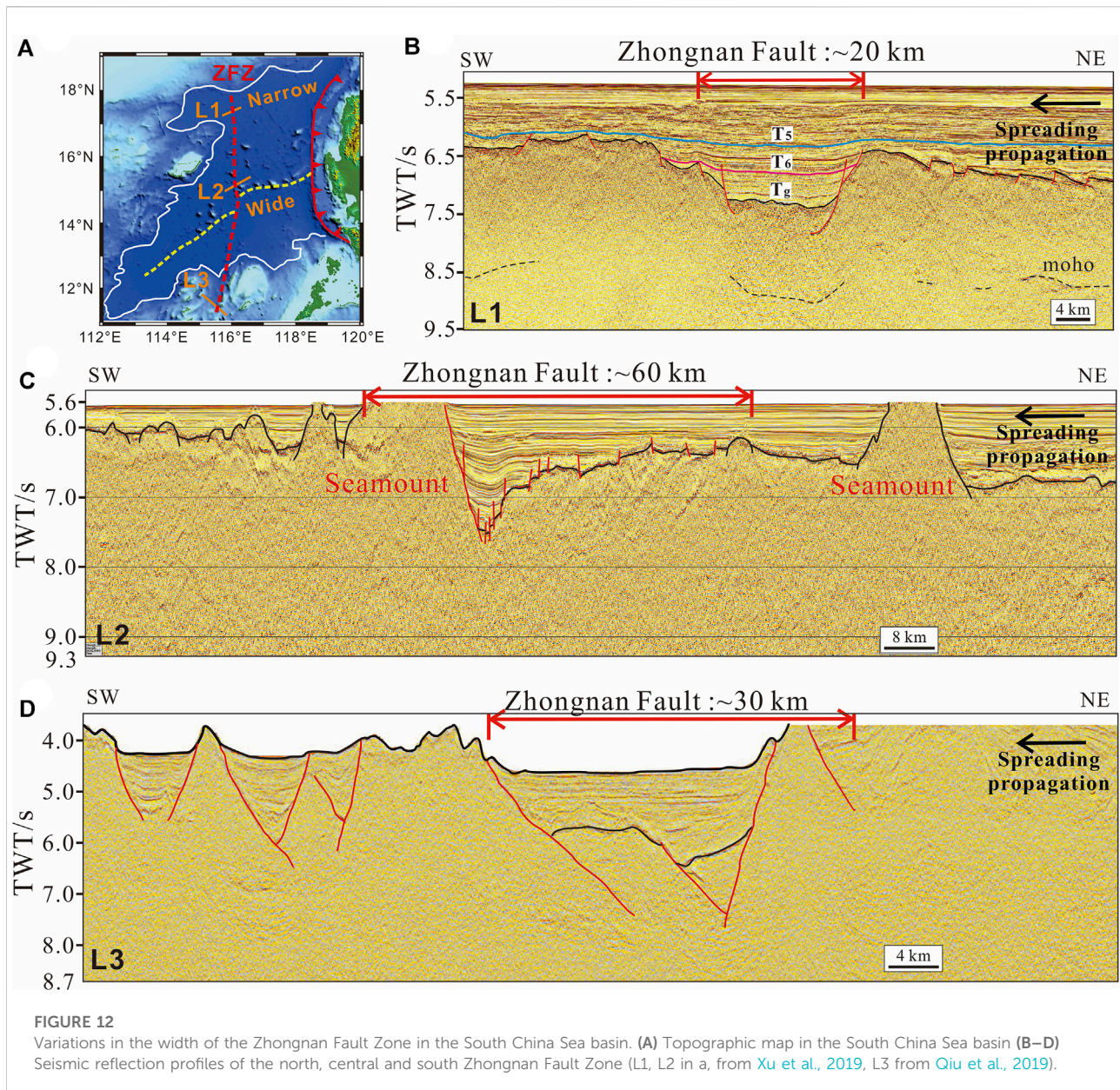
The initial orientation of the transform faults may influence rifting/spreading propagation. Based on the reference model with a pre-existing orthogonal transform fault, the models with obliquely distributed transform faults (i.e., rotated leftwards/rightwards by 30°) are further tested (Figure 9). Results show that model evolution differs largely from the reference model. 1) Firstly, the initially obliquely orientated transform faults fail to evolve to mature oceanic transform faults. Instead, the oblique transform faults experience intensive extension, forming inclined spreading ridges (Figures 9A, B). 2) Secondly, two ridge segments are formed in these models. However, unlike the reference model that ridge segments are connected to the transform fault, overlapping ridge segments are established in these models with the rotation of the

microplate in between (Figures 7C, D). The resulted overlapping ridge segments reflect strong interaction of the oblique transform faults on rifting/spreading propagation.

Discussion

Transform fault evolution affected by rifting/spreading propagation

The evolution of the pre-existing transform fault is also affected by rifting/spreading propagation. 1) Along the strike of the transform fault, two small-scale mantle convection cells are developed beneath the transform fault, with upwelling in the middle and downwelling at the ends (Figure 10C). These two convection cells are asymmetric and the one locates closer to the extensional boundary is more intense (Figure 10D). As a consequence to the upwelling/downwelling, decompressional melting and material dripping are formed in the middle and at the ends of the transform fault, respectively. Thus, the growth of the transform fault (i.e., increase of its length) is mainly due to the extension in the middle. The two ends of the transform fault are mainly under compression. 2) Perpendicular to the strike of the transform fault, cross sections reveal the variation of transform fault width. Ahead of the propagating ridge, the middle part of the transform fault becomes much wider, due to asthenospheric mantle upwelling triggered by ridge propagation. The southern end of the transform fault becomes



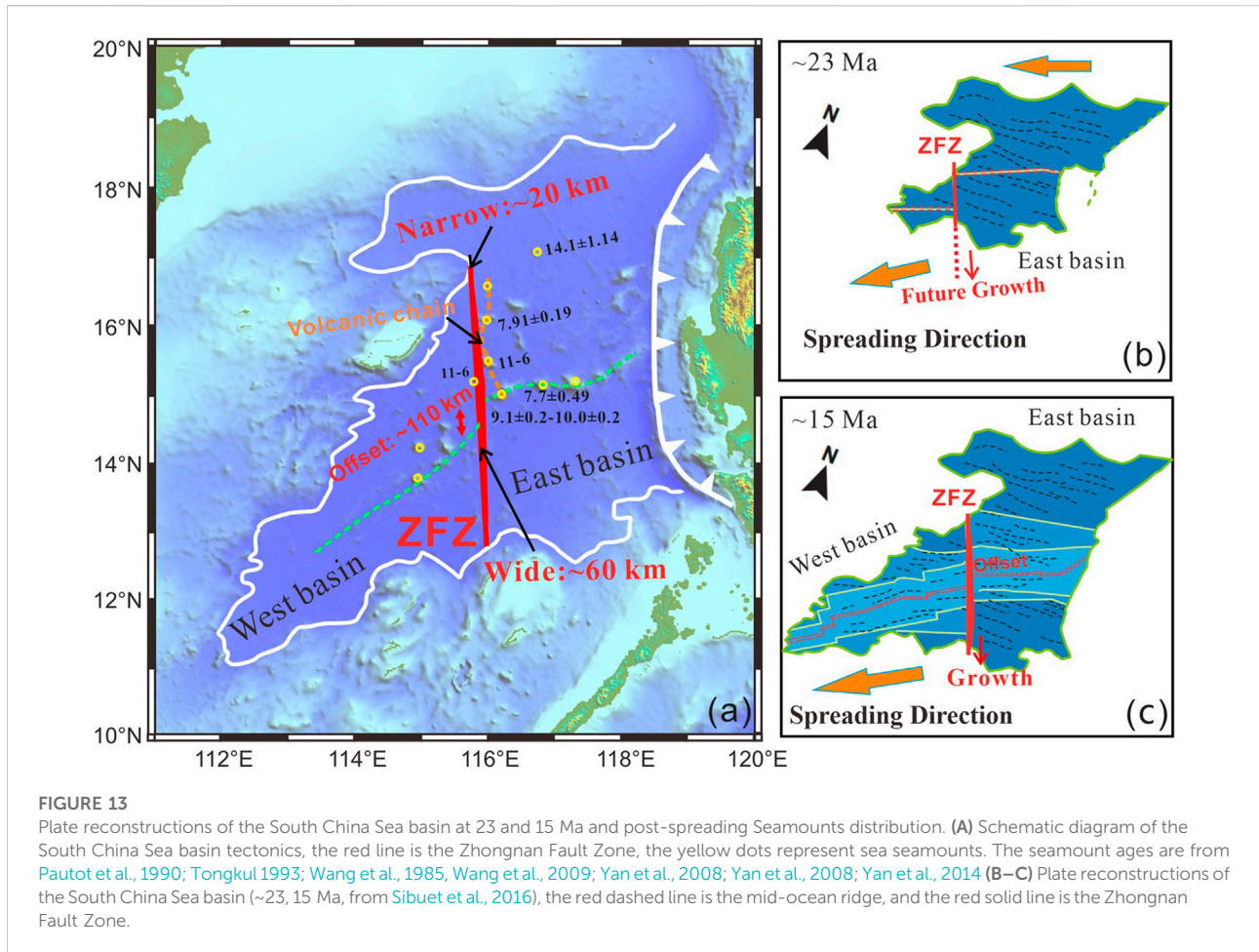
wider than the northern end, mainly because the transform fault grows to the south affected by the prescribed boundary extension (Figures 10E, F). Fault growth at the northern end is negligible, with very minor influence from the two ridge segments.

Besides, evolution of the transform fault is characterized by the formation of a volcanic chain (Figure 11A) due to the punctuated distribution of decompressional melting along the strike of the transform fault (Figure 11B). The volcanic chain is thus the surface expression of the deep discontinuous melting centers (Figure 10A). The deep discontinuous melting centers appear first in the middle of the transform fault (Figure 11B), and then establish at the southern end of the fault (Figure 11C), and finally migrate southward with the growth of the transform fault

(Figure 11D). The discontinuous randomly distributed melting centers along the transform fault are caused by the small-scale mantle convection cells due to transtensional and tranpressional deformation as described above.

Implications for the spreading of the south China sea basin

Our model results are comparable to the observations of the South China Sea basin, in terms of the growth of transform faults, the formation of ridge segments and the establishment of a volcanic chain. According to the fine interpretation of the seismic reflection



profiles in the South China Sea basin (Figure 12B), the Zhongnan Fault Zone cuts through the T6 horizon as well as the Tg horizon, but does not cut through the T5 horizon (where T5, T6 and Tg represents the early Miocene interface, the late Oligocene interface, and the early Oligocene basement, respectively), indicating that the Zhongnan Fault Zone was active before the early Oligocene-prior to the spreading of the South China Sea basin (~32 Ma; e.g., Li, 2012; Xu et al., 2019). This supports that the Zhongnan Fault Zone was a continental transform fault which evolved to an oceanic transform fault before and after the South China Sea basin spreading.

Firstly, the dynamic growth of the transform fault modeled in our study is comparable to the Zhongnan Fault Zone in the South China Sea basin (Figure 12; Xu et al., 2019; Barckhausen and Roeser, 2004, Barckhausen et al., 2014; Frank, 2013; Frank et al., 2004; Ruan et al., 2016; Sibuet et al., 2016). 1) The Zhongnan Fault Zone is 15–25 km wide at its northern end (Figure 12B), 60 km wide in the middle (Figure 12C) and ~35 km wide in the southern end (Figure 12D) revealed by seismic reflection data (Ruan et al., 2016; Qiu et al., 2019; Xu et al., 2021). Our model results are consistent with this phenomenon (Figure 10), and the increased width of the Zhongnan Fault in its middle, as suggested by our model results,

is likely caused by asthenospheric mantle upwelling ahead of the propagated spreading ridge. 2) The length of the Zhongnan Fault increased with the extension of the South China Sea basin. According to the plate reconstruction of the South China Sea basin (Briais et al., 1993) and the relative positions of the Zhongsha block and the Liyue-North Palawan micro-continent (Li, 2011), the Zhongnan Fault has been continuously growing southward with the significant increase in its length (Yan et al., 2014; Li et al., 2017). Our model results of transform fault growth are thus consistent with this observation.

Secondly, the formation of ridge segments with an offset distance is a remarkable feature of the South China Sea basin. Seafloor spreading in the southwest sub-basin of the South China Sea initiated at the south end of the Zhongnan Fault Zone, and propagated from east to west since 23.8 Ma (Figure 13B). An offset distance of ~110 km is formed between the two ridge segments in the east and southwest sub-basins (Figure 13A). Our model results are consistent with this phenomenon and indicate that the Zhongnan Fault Zone facilitated strain localization and promoted the formation of the ridge segment in the southwest sub-basin.

Thirdly, the lineated volcanic chain is observed along the Zhongnan Fault Zone in the South China Sea basin (Figure 13A).

According to our model results, formation of the lineated volcanic chain is likely related to the extensional deformation along the transform fault (Figure 11A). The reported ages of the volcanos from the volcanic chain along the Zhongnan Fault Zone were younger than the termination of the South China Sea basin spreading (Wang et al., 1985; Wang et al., 2009; Pautot et al., 1990; Tongkul 1993; Yan et al., 2008; Yan et al., 2008; Yan et al., 2014), indicating post-spreading magmatism. Whether there were older magmatic events along the Zhongnan Fault Zone remains enigmatic and need to be explored in the future.

The uplifting elevated topography and Moho surface of the transform fault suggested revealed by our models are observed at the Zhongnan Fault Zone, where there is only 8–10 km crust left and high values of gravity anomaly features (Ruan et al., 2016; Jourdon et al., 2020). In addition, a linear post-spreading seamount chain developed along the Zhongnan Fault Zone (Li et al., 2017; Xu et al., 2021), which indicates thin lithosphere and upwelling of hot asthenospheric underneath the fault zone. These observations suggest that the Zhongnan Fault Zone may have interacted with the spreading ridge of the east subbasin and experienced stages of extension. However, the Zhongnan Fault Zone/transform fault has only been discussed in earlier studies for its morphology, dynamic evolution and deep structure, its influence on sea floor spreading is not fully investigated (Barckhausen et al., 2004; Frank et al., 2004; Frank, 2013; Barckhausen et al., 2014; Ruan et al., 2016; Sibuet et al., 2016). Our results suggest that transform faults perpendicular to mid-ocean ridges have a significant influence on the spreading processes and evolution of ocean basins (e.g., North Iceland, Karson et al., 2019). The interaction with the oceanic spreading meanwhile leads to faults growth in its width and length. Brune et al., 2014, Clauser and Huenges, 1995, Gerya, 2010, Glerum et al., 2020, Gudmundsson et al., 2007, Guo et al., 2019, Huang et al., 2014, Lei et al., 2020, Li et al., 2011, Li et al., 2018, Li et al., 2019, Liao and Gerya, 2015, Karson et al., 1984, Ranalli, 1995, Ros et al., 2017, Taylor and Hayes, 1980, Wang et al., 2022.

Conclusion

We conducted a systematic study to investigate the interaction between pre-existing transform faults and rifting/spreading propagation using 3D dynamical numerical simulations. The main conclusions are given below:

- 1) The pre-existing transform faults affect rifting/spreading propagation promoting the formation of ridge segments with offset distances. The formation and development of the younger ridge segment is promoted by the pre-existing transform faults. Evolution of the pre-existing transform faults is also affected by spreading propagation featured by fault widening with melting and fault growth with increased length.
- 2) The initial length and orientation of the pre-existing transform faults affect rifting/spreading propagation,

controlling the offset distance between the ridge segments and the formation of overlapping ridge segments.

- 3) Our model results are comparable with natural observations in the South China Sea basin, in terms of the formation of offset ridge segments and transform fault evolution. We suggest that the pre-existing Zhongnan fault zone interacted rifting/spreading propagation and regulated seafloor spreading of the South China Sea basin.

Data availability statement

The raw data supporting the conclusions of this article will be made available by the authors, without undue reservation.

Author contributions

HL and JL designed the study. HL wrote the manuscript. YS, JQ and YW improve the manuscript. ZZ and XS helped to improve the manuscript with some suggestions. All authors contributed to the article and approved the submitted version.

Funding

This research is financially supported by NSFC projects (U1901214, 41974104, 91855208, 42109043) and the Guangdong project 2017ZT07Z006.

Acknowledgments

We thank Taras Gerya for his long-lasting guidance on our geodynamical modeling. We thank Linfeng Liao and Hao Su for their constructive suggestions. Numerical simulations were run with the clusters of National Supercomputer Center in Guangzhou (Tianhe-II). We would like to thank Ziyang Xu and Ning Qiu for their fine seismic profile results.

Conflict of interest

The authors declare that the research was conducted in the absence of any commercial or financial relationships that could be construed as a potential conflict of interest.

Publisher's note

All claims expressed in this article are solely those of the authors and do not necessarily represent those of their

affiliated organizations, or those of the publisher, the editors and the reviewers. Any product that may be evaluated in this article, or claim that may be made by its manufacturer, is not guaranteed or endorsed by the publisher.

References

- Bai, Y., Wu, S., Liu, Z., Müller, R., Williams, S., Zahirovic, S., et al. (2015). Full fit reconstruction of the South China Sea conjugate margins. *Tectonophysics* 661, 121–135. doi:10.1016/j.tecto.2015.08.028
- Barckhausen, U., Engels, M., Franke, D., Ladage, S., and Pubellier, M. (2014). Evolution of the South China Sea: Revised ages for breakup and seafloor spreading. *Mar. Petroleum Geol.* 58, 599–611. doi:10.1016/j.marpetgeo.2014.02.022
- Barckhausen, U., and Roeser, H. (2004). “Seafloor spreading anomalies in the South China sea revisited,” in *Continent-Ocean interactions within east asian marginal seas*. Editors P. Clift, W. Kuhnt, P. Wang, and D. Hayes (Washington, DC: AGU), 121–125. doi:10.1029/92jb02280
- Briaïs, A., Patriat, P., and Tapponnier, P. (1993). Updated interpretation of magnetic anomalies and seafloor spreading stages in the south China Sea: Implications for the Tertiary tectonics of Southeast Asia. *J. Geophys. Res.* 98 (B4), 6299–6328. doi:10.1029/92jb02280
- Brune, S., Heine, C., Pérez-Gussinyé, M., and Sobolev, S. (2014). Rift migration explains continental margin asymmetry and crustal hyper-extension. *Nat. Commun.* 5, 4014. doi:10.1038/ncomms5014
- Burg, J., and Gerya, T. (2005). The role of viscous heating in Barrovian metamorphism of collisional orogens; thermomechanical models and application to the Lepontine Dome in the Central Alps. *J. Metamorph. Geol.* 23 (2), 75–95. doi:10.1111/j.1525-1314.2005.00563.x
- Burov, E., and Cloetingh, S. (1997). Erosion and rift dynamics: New thermomechanical aspects of post-rift evolution of extensional basins. *Earth Planet. Sci. Lett.* 150 (1–2), 7–26. doi:10.1016/s0012-821x(97)00069-1
- Clauser, C., and Huenges, E. (1995). Thermal conductivity of rocks and minerals. *Rock Phys. Phase Relat. A Handb. Phys. Constants* 3, 105–126.
- Courtillot, V. (1982). Propagating rifts and continental breakup. *Tectonics* 1 (3), 239–250. doi:10.1029/TC001i03p0239
- Cramer, F., Schmeling, H., Golabek, G., Duretz, T., Orendt, R., Buitter, S., et al. (2012). A comparison of numerical surface topography calculations in geodynamic modelling: An evaluation of the ‘sticky air’ method. *Geophys. J. Int.* 189 (1), 38–54. doi:10.1111/j.1365-246X.2012.05388.x
- Franke, D., Dimitri, S., Manuel, P., Stephan, S., Benoit, M., Jean-Luc, A., et al. (2004). The final rifting evolution in the South China Sea. *Mar. Petroleum Geol.* 58, 704–720. ISSN 0264-8172. doi:10.1016/j.marpetgeo.2013.11.020
- Franke, D. (2013). Rifting, lithosphere breakup and volcanism: Comparison of magma-poor and volcanic rifted margins. *Mar. Petroleum Geol.* 43, 63–87. 0264-8172. doi:10.1016/j.marpetgeo.2012.11.003
- Gerya, T. V. (2010). *Introduction to numerical geodynamic modeling*. Cambridge University Press. doi:10.1017/CBO9780511809101
- Gerya, T. V. (2013). Three-dimensional thermomechanical modeling of oceanic spreading initiation and evolution. *Phys. earth Planet. interiors* 214, 35–52. doi:10.1016/j.pepi.2012.10.007
- Gerya, T. V., and Yuen, D. A. (2003). Rayleigh-Taylor instabilities from hydration and melting propel “cold plumes” at subduction zones. *Earth Planet. Sci. Lett.* 212 (1–2), 47–62. doi:10.1016/s0012-821x(03)00265-6
- Glerum, A., Brune, S., Stamps, D., and Strecker, M. (2020). Victoria continental microplate dynamics controlled by the lithospheric strength distribution of the East African Rift. *Nat. Commun.* 11 (1), 2881. doi:10.1038/s41467-020-16176-x
- Gudmundsson, A., Jacoby, W. R., and Gudmundsson, M. T. (2007). Infrastructure and evolution of ocean-ridge discontinuities in Iceland. *J. Geodyn.* 43 (1), 6–29. doi:10.1016/j.jog.2006.09.002
- Guo, L., Gao, R., Shi, L., Huang, Z., and Ma, Y. (2019). Crustal thickness and Poisson’s ratios of South China revealed from joint inversion of receiver function and gravity data. *Earth Planet. Sci. Lett.* 510, 142–152. doi:10.1016/j.epsl.2018.12.039
- Hey, R., Duennebier, F. K., and Morgan, W. J. (1980). Propagating rifts on midocean ridges. *J. Geophys. Res.* 85 (B7), 3647–3658. doi:10.1029/JB085iB07p03647
- Huang, H., Guo, X., Xia, S., and Qiu, X. (2014). Crustal thickness and Poisson’s ratio in the coastal areas of South China[J]. *Chin. J. Geophys.* 57(12): 3896–3906. (in Chinese). doi:10.6038/cjg20141204
- Illsley-Kemp, F., Bull, J. M., Keir, D., Gerya, T., Pagli, C., Gernon, T., et al. (2018). Initiation of a proto-transform fault prior to seafloor spreading. *Geochem. Geophys. Geosyst.* 19 (12), 2018GC007947–4756. doi:10.1029/2018GC007947
- Jourdon, A., Le Pourhiet, L., Mouthereau, F., and May, D. (2020). Modes of propagation of continental breakup and associated oblique rift structures. *J. Geophys. Res. Solid Earth* 125, e2020JB019906. doi:10.1029/2020JB019906
- Karson, J. A., Fox, P. J., Crane, K. T., Kidd, W. S. F., Bonatti, E., et al. (1984). The geology of the Oceanographer Transform: The ridge-transform intersection. *Mar. Geophys. Res. (Dordr.)* 6, 109–141. doi:10.1007/BF00285956
- Karson, J., Brandsdóttir, B., Einarsson, P., Sæmundsson, K., Farrell, J., and Horst, A. (2019). Evolution of migrating transform faults in anisotropic oceanic crust; examples from Iceland. *Can. J. Earth Sci.* 56 (12), 1297–1308. doi:10.1139/cjes-2018-0260
- Le Pourhiet, L., Chamot-Rooke, N., Delescluse, M., May, D. A., Watremez, L., and Pubellier, M. (2018). Continental break-up of the South China Sea stalled by far-field compression. *Nat. Geosci.* 11 (8), 605–609. doi:10.1038/s41561-018-0178-5
- Le Pourhiet, L., May, D., Huille, L., Watremez, L., and Leroy, S. (2017). A genetic link between transform and hyper-extended margins. *Earth Planet. Sci. Lett.* 465, 184–192. doi:10.1016/j.epsl.2017.02.043
- Lei, C., Alves, T., Ren, J., and Tong, C. (2020). Rift structure and sediment infill of hyperextended continental crust: Insights from 3D seismic and well data (xisha trough, south China sea). *J. Geophys. Res. Solid Earth* 125, e2019j-018610. doi:10.1029/2019jb018610
- Li, C., and Song, T. (2012). Magnetic recording of the Cenozoic oceanic crustal accretion and evolution of the South China Sea basin. *Chin. Sci. Bull.* 57, 3165–3181. doi:10.1007/s11434-012-5063-9
- Li, C., Xu, X., Lin, J., Sun, Z., Zhu, J., Yao, Y., et al. (2014). Ages and magnetic structures of the South China Sea constrained by deep tow magnetic surveys and IODP Expedition 349. *Geochem. Geophys. Geosyst.* 15, 4958–4983. doi:10.1002/2014GC005567
- Li, C., Zhou, Z., Li, J., Chen, B., and Geng, J. (2008). Magnetic zoning and seismic structure of the South China Sea ocean basin. *Mar. Geophys. Res. (Dordr.)* 29, 223–238. doi:10.1007/s11001-008-9059-4
- Li, F., Sun, Z., Pang, X., Liao, J., Yang, H., Xie, H., et al. (2019). Low-viscosity crustal layer controls the crustal architecture and thermal distribution at hyperextended margins; modeling insight and application to the northern South China Sea margin. *Geochem. Geophys. Geosyst.* 20 (7), 3248–3267. doi:10.1029/2019gc008200
- Li, F., Sun, Z., and Yang, H. (2018). Possible spatial distribution of the Mesozoic volcanic arc in the present-day South China Sea continental margin and its tectonic implications. *J. Geophys. Res. Solid Earth* 123 (8), 6215–6235. doi:10.1029/2017jb014861
- Li, J., Ding, W., Gao, J., Wu, Z. Y., and Zhang, J. (2011). Cenozoic evolution model of the sea-floor spreading in south China sea: New constraints from high resolution geophysical data[J]. *Chin. J. Geophys.* 54(12): 894–906. doi:10.1002/cjg2.1672in Chinese with English abstract
- Li, J. (2011). Dynamics of the continental margins in south China sea: Scientific experiments and research progresses. *Chin. J. Geophys.* 54 (12), 883–893. doi:10.1002/cjg2.1671
- Li, Y., Liu, H., Zhu, R., Wang, Y., Zhou, Y., and Xu, Z. (2017). Extension of the zhongnan-siling Fault Zone in south China sea and its bearing on seafloor spreading [J]. *Mar. Geol. Quat. Geol.*, 37(2): 82–98. In Chinese. doi:10.16562/j.cnki.0256-1492.2017.02.009
- Liao, J., and Gerya, T. (2015). From continental rifting to seafloor spreading: Insight from 3D thermo-mechanical modeling. *Gondwana Res.* 28 (4), 1329–1343. doi:10.1016/j.gr.2014.11.004

Supplementary material

The Supplementary Material for this article can be found online at: <https://www.frontiersin.org/articles/10.3389/feart.2022.1054747/full#supplementary-material>

- Müller, R. D., Seton, M., Zahirovic, S., Williams, S. E., Matthews, K. J., Wright, N. M., et al. (2016). Ocean basin evolution and global-scale plate reorganization events since Pangea breakup. *Annu. Rev. Earth Planet. Sci.* 44, 107–138. doi:10.1146/annurev-earth-060115-012211
- Patout, G., Rangin, C., Briais, A., Wu, J. L., Han, S. Q., Li, H. X., et al. (1990). The axial ridge of the South China sea: A seabeam and geophysical survey. *Oceanol. Acta* 13 (2), 129–143.
- Qiu, N., Yao, Y., Zhang, Y., et al. (2019). Characteristics of the crustal and its tectonic significance of the continental margin of SE South China Sea. *Chin. J. Geophys.* 62 (7), 2607–2621. in Chinese.
- Ranalli, G. (1995). *Rheology of the Earth*. Springer Science & Business Media.
- Ros, E., Perez-Gussinye, M., Araujo, M., Thoaldo Romeiro, M., Andres-Martinez, M., and Morgan, J. P. (2017). Lower crustal strength controls on melting and serpentinization at magma-poor margins: Potential implications for the South Atlantic. *Geochem. Geophys. Geosyst.* 18, 4538–4557. doi:10.1002/2017GC007212
- Ruan, A., Wei, X., Niu, X., Zhang, J., Dong, C., Wu, Z., et al. (2016). Crustal structure and fracture zone in the Central Basin of the South China Sea from wide angle seismic experiments using OBS. *Tectonophysics* 688, 1–10. ISSN 0040-1951. doi:10.1016/j.tecto.2016.09.022
- Sibuet, J. C., Yeh, Y. C., Lee, C. S., et al. (2016). Geodynamics of the South China sea. *Tectonophysics* 692, 98–119. doi:10.1016/j.tecto.2016.02.022
- Taylor, B., and Hayes, D. E. (1980). “The tectonic evolution of the South China Sea Basin” in *The tectonic and geologic evolution of South East Asian Seas and Islands*. Editor D. E. Hayes. *Geophys. Monogr. Ser. 27* (Washington, DC: AGU), 23–56. doi:10.1029/GM023p0089
- Tongkul, F. (1993). Tectonic control on the development of the neogene basins in sabah, east Malaysia[C]. Proceedings Symposium on the Tectonic Framework and Energy Resources of the Western Margin of the Pacific Basin. Kuala Lumpur, Malaysia. Geological Society of Malaysia. 95–103. November 1993. doi:10.7186/bgsm33199307
- Vink, G. E. (1982). Continental rifting and the implications for plate tectonic reconstructions. *J. Geophys. Res.* 87 (13), 10677–10688. doi:10.1029/JB087iB13p10677
- Wang, X., Wu, M., Liang, D., and Yin, A. (1985). Some geochemical characteristics of basalts in the South China Sea. *Chin. J. Geochem.* 4 (4), 380–390. doi:10.1007/bf02843275
- Wang, Y., Han, X., Luo, Z., Qiu, Z., Ding, W., Li, J., et al. (2009). Late Miocene magmatism and evolution of zhenbei-huangyan seamount in the South China sea: Evidence from petrochemistry and chronology. *Acta Oceanol. Sin.* 283 (5747), 532–537. in Chinese with English abstract. doi:10.1038/283532a0
- Wang, Z., Singh, S. C., Prigent, C., Gregory, E. P. M., and Marjanovic, M. (2022). Deep hydration and lithospheric thinning at oceanic transform plate boundaries. *Nat. Geosci.* 15, 741–746. doi:10.1038/s41561-022-01003-3
- Xu, Z., Wang, J., Gao, H., Sun, G., Sun, M., Nie, X., et al. (2019). Research progress on the zhongnan-liyue Fault Zone in the South China Sea Basin*[J]. *J. Trop. Oceanogr.* 38(2): 86–94. In Chinese with English Abstract.
- Xu, Z., Wang, J., Yao, Y., Tang, J., Gao, H., and Li, X. (2021). The temporal-spatial distribution and deep structure of the zhongnan- liyue Fault Zone in the north of the South China Sea Basin. *Earth Sci.* 46 (3), 942–955. In Chinese with English Abstract. doi:10.3799/dqkx.2020.400
- Yan, Q., Shi, X., and Castillo, P. R. (2014). The late mesozoic–cenozoic tectonic evolution of the South China sea: A petrologic perspective. *J. Asian Earth Sci.* 85 (2), 178–201. doi:10.1016/j.jseas.2014.02.005
- Yan, Q., Shi, X., Wang, K., Bu, W., and Xiao, L. (2008). Major element, trace element, and Sr, Nd and Pb isotope studies of Cenozoic basalts from the South China Sea. *Sci. China Ser. D-Earth. Sci.* 51 (4), 550–566. doi:10.1007/s11430-008-0026-3
- Yan, Q., Shi, X., Yang, Y., and Wang, K. (2008). Potassium-argon/argon-40-argon-39 geochronology of Cenozoic alkali basalts from the South China Sea. *Acta Oceanol. Sin.* 27 (6), 115–123.